Title
Simulations of the dissociation of small helium clusters with ab initio molecular dynamics in electronically excited states.

Journal
The Journal of chemical physics, 140(13)

ISSN
0021-9606

Authors
Closser, Kristina D
Gessner, Oliver
Head-Gordon, Martin

Publication Date
2014-04-01

DOI
10.1063/1.4869193

Peer reviewed

Simulations of the dissociation of small helium clusters with ab initio molecular dynamics in electronically excited states

Kristina D. Closser,[1,2] Oliver Gessner,[2] and Martin Head-Gordon[1,2,a)]

[1)] *Department of Chemistry, University of California: Berkeley, Berkeley CA*

[2)] *Ultrafast X-Ray Science Laboratory, Chemical Sciences Division, Lawrence Berkeley National Laboratory, Berkeley CA*

(Dated: 7 March 2014)

The dynamics resulting from electronic excitations of helium clusters were explored using *ab initio* molecular dynamics. The simulations were performed with configuration interaction singles (CIS) and adiabatic classical dynamics coupled to a state-following algorithm. 100 different configurations of He_7 were excited into the $2s$ and $2p$ manifold for a total of 2800 trajectories. While the most common outcome (90%) was complete fragmentation to 6 ground state atoms and 1 excited state atom, 3% of trajectories yielded bound, He_2^*, and $< 0.5\%$ yielded an excited helium trimer. The nature of the dynamics, kinetic energy release and connections to experiments are discussed.

[a)]Electronic mail: mhg@cchem.berkeley.edu

I. INTRODUCTION

The apparent, beautiful simplicity and unique properties of pure helium clusters attract ever increasing attention to their fundamental properties and potential applications.[1–7] Excited states of helium clusters are interesting from a basic science perspective, in particular, for the study of solvent-solute interactions such as energy- and charge-transfer between the superfluid helium matrix and dopant atoms and molecules.[3,6,8]

Despite a growing number of experimental and theoretical studies, it is only quite recently that the tools have become available for detailing the electronic structure of excited helium clusters and to follow their dynamic evolution.[8–13] Experimentally, generating sufficient energy (> 20 eV) for electronic excitations, the non-uniformity of the cluster sizes, and the multitude of simultaneously progressing dynamic channels pose significant challenges.[3,14] Recent work by the Berkeley Lab group has added greatly to the current understanding of electronically excited states and found, at least for large clusters, that excitations lead to different relaxation channels based on the energy and location of the initial excitation.[9–12] However, significant uncertainties remain on the mechanism of the excitation decay, especially at the atomic scale.

Theoretical studies of helium clusters have also been rather limited due to the inherent challenges in computing excited states of extended systems with many nearly degenerate states. Large scale semi-empirical models, such as the step potential model with hard sphere scattering,[11,12] and the liquid drop model,[3,15] do not contain any microscopic information and are not capable of capturing atomic level details. *Ab initio* dynamics of ground-state neutral[16,17] and ionized helium clusters[18] have been investigated, but dynamics in the excited states remain elusive. Our earlier work[19] on 7- and 25-atom clusters and that of von Haeften and Fink[20] on He_7 probed the vertically excited states of small helium clusters yielding insight at the atomic level for static states. However, these did not account for any dynamics resulting from the initial excitation.

Treating both the nuclei and electrons quantum mechanically rapidly becomes intractable as the system size grows. Thus, most *ab initio* molecular dynamics (AIMD) calculations rely on mixed quantum-classical methods where the nuclei are propagated classically and the electrons quantum mechanically on a single state of the system. Adiabatic or Born-Oppenheimer AIMD of ground electronic states has an extensive history and can be a useful

tool for studying non-stationary systems.[21,22] This method does not require any foreknowledge of the behavior of the system, and the adiabatic approximation is generally valid as long as the Born-Oppenheimer approximation holds. Near conical intersections and avoided crossings, the motion of nuclei and electrons cannot be straightforwardly separated and the adiabatic picture breaks down.

Attempts to expand AIMD to excited states and non-adiabatic dynamics have met with varying degrees of success.[23–30] The most common methods for contending with interacting potential surfaces, which give rise to non-adiabatic transitions, are variations of Tully's surface hopping.[31–33] Surface hopping algorithms probabilistically allow switching between surfaces and necessarily involve large numbers of trajectories for each initial state. They also lack a fully rigorous derivation, and are especially problematic when multiple nearly degenerate regions exist or when passing through more than one interaction region.[34,35] Alternative methods for computing molecular dynamics involve following the excited state Born-Oppenheimer (adiabatic) surface, transforming to a diabatic representation, and Ehrenfest (mean-field) dynamics[36]. All of these also have their weaknesses. Purely Born-Oppenheimer dynamics often do not give physically relevant results,[37] converting to diabatic representations is not entirely well defined,[38,39] and Eherenfest dynamics are not microscopically reversible.[36]

Our primary interest here is to determine the fate of helium cluster excitations. Since the excitations are into a dense manifold of states it is impractical to run statistically relevant numbers of trajectories in all possible states. Thus, we have adopted a slightly different approach and use a deterministic algorithm, which is similar to Born-Oppenheimer dynamics much of the time, but preferentially follows the diabatic state when near-degeneracies occur. A single trajectory for each excited state is launched with zero kinetic energy, which implies that all kinetic energy developed during the course of the trajectory is a direct result of the forces exerted by the excited state. After the initial excitation, a recently developed state following algorithm selects the subsequent state based on the character and energy of the previous state.[40]

The high cost of calculating trajectories "on the fly" dictates the underlying electronic structure method be as efficient as possible. For excited states, time-dependent density functional theory (TDDFT) is often the best option. It is efficient and can give very good results, provided the functional is chosen carefully.[25,26,30] Wavefunction based methods may

also be attractive in some cases as they generally have more predictable errors. However, with the notable exceptions of configuration interaction singles (CIS) and time-dependent Hartree-Fock (TDHF), they are computationally more demanding.[23,27,28] For most systems CIS and TDHF yield poorer results than TDDFT due to the lack of electron-correlation, but in certain circumstances the may be preferable. One such instance is with Rydberg states that suffer from self-interaction error for standard density functionals.[41,42]

Previously, we reported[19] theoretical studies on the static excited states of small clusters (He_n, $n = 7, 25$) for $2s$ and $2p$ excited states. It was found that a good description of the excited states could be obtained using comparatively cheap CIS calculations and that the excitation depth, at least for the $2s$ and $2p$ states, correlated strongly with the blue shift of the excitation. Here, we investigate the fate of He_7 excitations by AIMD coupled with state following, and present the results of atomically resolved dynamics for relaxation of He_7^* clusters excited initially into the $n = 2$ manifold (< 23 eV).

II. METHODS

We compute helium cluster excited states using configuration interaction singles (CIS) and use standard Born-Oppenheimer dynamics coupled with a state-following algorithm to determine their fates. The overlap of the attachment and detachment densities from nearby excited states assesses their character and determines their population from the current state when near degeneracies occur. All calculations run on a single processor using a developmental version of Q-Chem 4.0[43].

A. Geometries

We generate the initial cluster geometries as in our previous work[19]. A random distance between 0 and 3 Å is added to the x, y, and z coordinates of each atom in a 3 Å octahedral cluster[44]. The randomized cluster is then optimized using MP2 with a standard Pople 6-311G basis set. Due to the extremely shallow potential well, a myriad of local minima with similar energies exist, and no duplicate geometries occurred for 100 such clusters. The spread of the ground state MP2 energies for the optimized clusters is 6 meV, which is extremely small relative to the excitation energies $\gtrsim 21$ eV, and the errors in CIS are

generally far larger than this difference. The average inter-atomic distance for He_7 clusters generated using this randomization procedure is 3.7 Å, which is very close to the previously determined pair-distribution function result of 3.60 Å for much larger clusters.[45,46] Selecting only the absolute nearest-neighbor distance for each initial geometry yields an average of 3.0 Å, which also correlates very closely to the large cluster nearest-neighbor distance of ≈ 3.05 Å.[45,46]

In such small clusters the definition of surface and bulk states is ill-defined. The surface region for large, finite clusters may be defined by the variation of the bulk value, which, for large helium droplets (He_N, $N \geq 1000$), is ≈ 6 Å thick.[3,47] The absolute largest interatomic distance in the model systems presented here was 7.6 Å, and thus these calculations do not include bulk effects. However, microscopic dynamics in large helium clusters are frequently discussed considering local atom-atom interactions in which the droplet environment surrounding an excited atom is represented either by an average potential or by a single nearest neighbor atom.[11,15,48–50] The dynamics simulations presented here offer an opportunity to extend this picture to a quantitative description of excitations and interactions including virtually all nearest neighbor atoms of an excited cluster moiety. This approach may provide valuable benchmarks, in particular, to guide the interpretation of experiments that provide increasing evidence for marked differences between dynamics proceeding in the bulk and surface regions of large helium clusters.[11,12,51,52]

B. Vertical excitations

The excited state energies and forces are calculated with CIS[53,54] in the 6-311(2+)G Pople basis. This is the standard 6-311G basis supplemented with two sets of diffuse functions and is the smallest basis yielding qualitatively good results for the $n = 2$ excitation manifold. The first set of diffuse functions uses the coefficients from Yin and MacKerell[55], and the second set results from scaling the exponents of the first by 1/3.32.[19] CIS is among the lowest scaling *ab initio* methods for excited states and, for small helium clusters, gives results qualitatively similar to higher level wavefunction methods such as equation of motion coupled-cluster singles and doubles (EOM-CCSD).[19,56] Contrasted with single-point calculations, the impact of computational cost increases dramatically for trajectory calculations, therefore a low-scaling method is crucial for AIMD calculations. The density functional equivalent of CIS is

the Tamm-Dancoff approximation to TDDFT.[57–59] However, self-interaction error is an issue with standard density functionals when computing diffuse Rydberg states so a wavefunction based method is preferred in this instance.[41,42]

In addition to the energy, when performing dynamics simulations the electronic gradient of the excited state will also be crucial. To asses whether the CIS forces were reasonable we also computed the initial forces using EOM-CCSD. The average magnitude of the CIS forces is 0.036 eV/Å and for EOM-CCSD is 0.041 eV/Å. Subtracting the EOM-CCSD gradient from the CIS gradient component-wise and then evaluating the magnitude of the difference gave a root mean square deviation of 0.002 eV/Å. Thus, the CIS forces are slightly smaller in magnitude (99% confidence).

C. Dynamics

Classical nuclear dynamics with a standard velocity-Verlet algorithm[60] propagate the nuclei. Each atom is initialized with zero velocity so that all kinetic energy (KE) developed during the course of the trajectory is due to excited state forces. The selection of the electronic state at each time-step is based on a newly developed algorithm that will be briefly described here and detailed in a forthcoming publication.[40]

We compute the AIMD trajectories using a step size of 5 a.u. ≈ 0.1 fs (1 a.u. $= 0.0242$ fs) for a minimum of 242 fs (2000 steps) and a maximum of 968 fs (8000 steps). In order to optimize computational resources, any time a trajectory clearly results in full fragmentation or reaches a stationary point, the calculation terminates. Cluster trajectories associated with partial fragmentation that do not stagnate are computed until the maximal time. The criteria we use for halting the trajectories are the magnitude of the electronic gradient at the current time step ($< 1 \times 10^{-4}\ E_h/a_o$), and either the difference in energy ($< 1 \times 10^{-8}\ E_h$) or the difference in magnitude of all atomic displacements ($< 1.2 \times 10^{-4}$ Å) between successive time steps. This produces essentially the same product distribution as if all trajectories were run to 968 fs.

All 28 singlet $n = 2$ vertically excited states are populated at t_0 and subsequent electronic states are selected based on energy and character. Most often this corresponds to simply following the adiabatic surface, but if multiple states exist very near each other the character of the nearby states is evaluated and the one with the most similar character is chosen

provided there is an obvious choice. Curve crossings in helium clusters with this method are quite rare events. The majority of the trajectories ($\approx 60\%$) experience 0 crossings and 90% have ≤ 10 crossings. Also, despite the high density of states there is rarely uncertainty about which state should be chosen. About 0.05% of the time steps had nearly degenerate states that could not be described well in terms of the character of the state from the previous time step. Of these uncertain steps, 40% result from basis set discontinuities, which can occur when atoms collide.

The definition of nearness to a given state k (energy E_k) is controlled by the user-set parameter γ_E such that all states n within the window $E_n < (E_k \pm \gamma_E)$ are accessible and $\gamma_E = 0$ corresponds to pure adiabatic dynamics. The estimated E_n for the current time step includes the energy of the previous state and the propagated kinetic energy. For helium clusters a value corresponding to $\gamma_E = 0.0005\ E_h$ (≈ 0.01 eV and roughly 0.5% of the $n = 2$ excited state band) is chosen. This window is sufficient to contain all nearly degenerate states while preventing erroneous switching into a state of a similar character but significantly different energy. The trajectory fates are relatively insensitive to this parameter. However, if chosen to be too large for the system (e.g. 0.5 eV), unphysical, non-energy conserving products can result. For example multiple dimers can form that have a total energy much higher than the initial excitation.

If no more than one state is predicted to be near state k at time t_i the state closest in energy is chosen for t_{i+1}. When multiple states may be accessed their attachment ($\mathbf{A}$) and detachment ($\mathbf{D}$) densities are compared to those of the previous state. This provides an overlap metric for the particle and hole densities which is not sensitive to phase instabilities.[61] A scale from 0-1 is used where a value of 0 indicates that both densities have no points in common and 1 correlates to states with identical densities at t_i and t_{i+1}. The magnitude of the difference density, $\mathbf{S} = 1 - \frac{1}{2}\left|\mathbf{A}_{t_{i+1}} - \mathbf{A}_{t_i} - (\mathbf{D}_{t_{i+1}} - \mathbf{D}_{t_i})\right|$, defines the similarity scale. To determine similar character a threshold of 50% ($\mathbf{S} \geq 0.5$) was used and the state with the largest overlap greater than this value was selected. The dynamics are also not highly sensitive to this threshold for a wide range of values and it primarily exists for other applications of this state-following algorithm, such as in excited-state geometry optimizations.[40] In the occasional instance where a time step did have an overlap below the γ_S the state following code defaulted to selecting the adiabatic state (nearest in energy). This uncertainty in state selection occurred in $\approx 0.05\%$ of the time steps and was often due to basis set discontinu-

ities (primarily when atoms collide) or when passing through a conical intersection where all states dramatically change character between time t_i and t_{i+1}.

State-switching was found to be quite a rare event. The majority (56%) of the trajectories had no changes, 87% had $\leq$ 5 and 90% had $\leq$ 10 state-switches. Furthermore, when considering all computed time steps (7.7×10^6) only 1.4×10^4 ($\leq$ 0.02%) steps had a state that changed from the previous step. Thus, this dynamics algorithm produces largely adiabatic trajectories, with state switches based on the excited-state character allowed only when more than one state occurs in a small energy window.

Trajectories were initialized on all helium $n = 2$ states accessible by single photon absorption. CIS does not allow changes in electron spin and helium has low spin-orbit coupling so triplet states are neglected and only singlet states are computed. In He_7 clusters, the seven lowest-energy states correspond to superpositions of $2s \leftarrow 1s$ atomic-like excitations and 8 through 28 correspond to superpositions of $2p \leftarrow 1s$. Conservatively, for $2s \leftarrow 1s$ and $2p \leftarrow 1s$ transitions, 14 states and 28 states respectively are calculated at each step along the trajectory. Energy conservation dictates the potential energy must decrease for any increase in KE so only states with potential energies lower than the initial excitation are ever accessible. A significant energy gap between the highest energy $n = 2$ state and the lowest $n = 3$ state prohibits crossing into a state with $n \geq 3$ for any initial excitations to the $n = 2$ manifold. Finally, even though by single photon excitation the p states are primarily populated, we consider all singlet $2s$ and $2p$ states for each of the 100 He_7 clusters as it is possible for a $2p$ state to undergo a non-radiative transition into a $2s$ state. Thus, a total of 2800 trajectories were computed.

III. RESULTS AND DISCUSSION

The density of states in the $n = 2$ singlet manifold is shown in fig. 1 for all 100 of the He_7 clusters. There are two distinct bands peaked at the atomic $2s$ and $2p$ states. While some mixing of states was observed in the vertical excitation, it was always fairly straightforward to classify the state as dominantly $2s-$ or $2p-$like ($\sigma-$ or $\pi-$like). This is due to the energy separation between the $s-$ and $p-$type states of helium. The bands are strongly skewed with blue shifted tails and the $n = 2$ manifold spans over 2 eV. Note that these are calculated with CIS/6-311(2+)G and are shifted by $\approx$ 0.6 eV from the generally accepted values.[62]

This constant shift is due to the error inherent to CIS and this finite basis,[19] and as we focus on qualitative effects the results are presented in their uncorrected form.

The single photon excitation spectrum is also given in the inset of fig. 1. It is estimated by weighting the density of states with the oscillator strengths. As expected from dipole selection rules, the p states strongly dominate in intensity, though there is a small contribution from $s-$type states due to s and p mixing. Trajectories are initiated in all states, although in single photon experiments the population of $2p$ states clearly dwarfs the $2s$ states.

Much information and some calibration of the expectations can be obtained by analyzing He_2 and so we begin there before detailing the results of the He_7 cluster dynamics.

A. Helium Dimer

In order to develop a qualitative intuition for the excited-state forces that drive nuclear motion during cluster relaxation, we first analyze the potential energy curves of helium dimers in the $n = 2$ Rydberg manifold. The potential curves were calculated using the same model chemistry that was used for the trajectory calculations, CIS/6-311(2+)G, so that we can directly apply the dimer results to what is expected using this method. Figure 2 shows the ground and first 8 excited states of the neutral dimer as well as the ground state of the cation, He_2^+.

The essentially unbound ground molecular state ($^1\Sigma_g$), dissociates into two $1s$ ground state atoms. Since He atoms contain two paired electrons in the filled $1s$ shell, the separated atoms are extremely stable and do not readily bond with each other. He_2 is completely unbound in the mean-field limit and must rely on dispersive forces to obtain its extremely shallow potential well.[63] This is also what one would predict from the textbook molecular orbital (MO) picture because the ground-state dimer has four electrons with equal numbers in bonding (1σ) and anti-bonding ($1\sigma^*$) orbitals.

The excited states of helium all necessarily involve higher principle quantum numbers, $n \geq 2$, and, contrasting with the ground state, some of the excited states exhibit regions of significant binding. Again, this can be predicted by basic MO theory; in the lowest excited states of He_2 an electron from a $1\sigma^*$ orbital is promoted to a bonding orbital (2σ or 2π). In atomic He^* the excited electron enters a diffuse Rydberg orbital and although it is neutral it may be interpreted as a positively charged He^+ core with a distant electron. Similarly,

excited states of the dimer behave as a He_2^+ core surrounded by a remote electron, though this trend does not obviously hold for larger excited clusters.[64,65] In He_2^+ the atoms are actually held together by electrostatic forces and thus He_2^* has a very stable bound core.

The lowest excited state dissociation limit is the doubly degenerate He($1s$)+He($2s$) which is followed by the sextuply degenerate He($1s$)+He($2p$). The fourth dissociation limit in fig. 2 results in ionized He^+($1s$)+He($1s$). In order to properly describe states with $n \geq 3$ a significantly larger basis is required and these states will not be discussed further.

At equilibrium, the first excited state is bound by just over 2 eV and has σ_s character. The second and third states are of π character resulting from the p_x and p_y atomic orbitals with one dissociating to atomic $1s+2s$ and the other to $1s+2p$. The σ_{p_z} state resulting from the p_z atomic orbitals is actually the fifth state when ordered energetically. It is significantly higher in energy than the other bonding states and also has a lower binding energy of 0.5 eV. The corresponding σ_s^*, $\sigma_{p_z}^*$ and doubly degenerate π^* are also shown in the figure. All of the asymptotically anti-bonding states have bonding character at short internuclear distances. The potential well minima lie at least ≈ 0.5 eV below the correlated dissociation limits, with the exception of $\sigma_{p_z}^*$, which is barely bound. A close inspection of fig. 2 reveals that the potential minimum of all He_2^* states occurs at 1.1 Å as does the He_2^+ ground state. This is consistent with interpreting He_2^* as a cationic core with a distant and diffuse excited electron.

At larger inter-atomic distances $\gtrsim 3$ Å, the excited states of the dimer are all very weakly attractive or repulsive. Of these 3/8 are attractive and tend towards the bound region, and 5/8 are repulsive resulting in fully-separated atoms. Thus we expect the majority of trajectories to dissociate, and those that do remain bound will likely contain significant vibrational energy.

Using a harmonic approximation the vibrational state spacing in both the ground state of He_2^+ and first exited state of He_2 is roughly 1600 cm^{-1}. This corresponds to a zero-point energy of ≈ 800 cm^{-1} and an oscillation period of approximately 21 fs. Fitting to a Morse potential reveals that vibrational states near the top of the well have periods over an order of magnitude longer. The π and σ_s excited states are the broadest and, thus, they are expected to support longer periods than other He_2^* states which have narrower and shallower wells.

B. Illustrative trajectories

Sample trajectories for He_7^* clusters are shown in fig. 3. Snapshots of the atoms every 1 fs are shown, with the final geometry given by the large (red) atoms. The most commonly observed outcome is full fragmentation into seven separate atoms one of which carries the electronic excitation, $He^* + 6$ He. In principle excited clusters from He_2^* to He_7^* can also be formed although only He_2^* and He_3^* are observed. In the dimer the majority of the excited states are weakly repulsive at interatomic distances that are characteristic of those found in the interior of large clusters (fig. 2). Thus, it may be expected that a He_7 cluster most commonly undergoes full dissociation after excitation, but we may also anticipate effects of attractive forces at short internuclear distances which give rise to complex relaxation dynamics.

1. Atomization

Two possible ways full fragmentation may occur include direct dissociation as illustrated by the trajectory in fig. 3a or involving collisions between atoms as shown in fig. 3b. This fragmentation is to six ground state atoms and one atom that is excited to a $2s$ or $2p$ state. The excitation localizes onto a single atom at large internuclear separations as the vertical excitation energy is not large enough to support multiple excited atoms.

Careful attachment and detachment analysis was performed for many individual trajectories. Figure 4 illustrates detachment (red) and attachment (blue) densities at various steps along the trajectory shown in fig. 3a. The initial excitation into a semi-delocalized $2s-$type orbital moves about the cluster before settling onto a single atom after ≈ 200 fs, where it remains for the duration of the trajectory. The two time steps in fig. 4d have slightly different atomic positions, but the excitation is qualitatively the same in both. Figure 5 shows the densities associated with the colliding trajectory of fig. 3b. Here, an initially delocalized $2p-$state localizes onto two atoms beginning around $t = 12$ fs (fig. 5b). This excited dimer then undergoes an elastic collision between 90 and 120 fs. The atoms do not remain together because the kinetic energy of their approach, which is not dissipated by interactions with additional atoms, is too high to allow bonding in this case. Ultimately, this cluster fully dissociates and results in a single $2s$ excited atom by ≈ 300 fs (fig. 5f).

2. Dimerization

Approximately 3% of all trajectories lead to the formation of stable, excited dimers. The dimers form with varying amounts of vibrational energy as illustrated by the trajectories in fig. 3c and fig. 3d. Longer periods of vibration usually, and for purposes of this study, always correspond to states with higher vibrational energy. As seen in fig. 2, for bound states the potential well broadens as the vibrational excitation increases and the corresponding decrease in the potential gradient leads to longer vibrational periods.

Figure 6 shows the detachment/attachment density evolution associated with the dimer forming trajectory of fig. 3d. Here, the initial excited state is a highly delocalized superposition of atomic $2p \leftarrow 1s$ states. At ≈ 120 fs some localization is observed, and by 240 fs the excitation has fully localized onto a single pair of atoms. Note that the apparent partial charge-transfer character (spatial separation of red and blue zones) of the state in of fig. 6b is an artifact due to the graphic representation of the isosurface; decreasing the contour value reveals the attachment density also surrounds the atom that appears to carry isolated detachment densities. In fig. 6c the dimer is in a π state that morphs into a σ^* state (fig. 6d) and back to a π state (fig. 6e). In this case it occurs through a series of non-adiabatic transitions. The vibronic oscillation of the excited dimer continues to the end of the 968 fs trajectory with an average period of 88.5 fs. The vibrational period of this dimer is long compared with that of the trajectory shown in fig. 3c indicating that different states of He_2^* are formed. The trajectory of fig. 3c also happens to form a π-state dimer, but with much lower vibrational energy. In addition to varying vibrational periods we also observed dimers in nearly all possible electronic states: σ_s, σ_s^*, π, π^*, and σ_{p_z}. Figure 7 shows sample attachment densities for each type of He_2^* electronic state at the final point of their respective trajectories.

3. Trimerization

Even more rarely, He_3^* fragments are detected. Figure 3e shows the formation of an excited trimer and fig. 8 shows the corresponding attachment and detachment densities. Here the state is initially more or less a localized $2p \leftarrow 1s$ atomic state with very small excitation amplitudes on neighboring atoms. The excitation then spreads until it is located

on two non-adjacent atoms separated by over 5 Å. Between 280 and 660 fs (figs. 8e to 8i) the excitation remains on the same two atoms and undergoes oscillations of the excited state density on a time scale of ≈ 100 fs. After 660 fs, the excitation spreads to the middle atom of the trimer and then remains on all three atoms for the duration of the trajectory (figs. 8j to 8l). The excitation does not appreciably spread over all three atoms until the distance between the central atom and each of the side atoms is less than ≈ 3 Å.

The excited trimer, He_3^*, is very weakly bound according to high-level theoretical calculations (2.27 mK ≈ 2×10^{-4} meV) and has not been observed experimentally.[66,67] The corresponding linear cation He_3^+, is strongly bound relative to 3 fully separated atoms but only weakly relative to He_2^+ + He. Careful calculations (CCSD(T)/aug-cc-pVQZ) have determined He_3^+ to be bound by 2.65 eV relative to the three-body dissociation limit and only by 0.29 eV relative to He_2^+ + He.[64] The CIS/6-311(2+)G values relevant for this work are 1.6 eV relative to 2He + He^+ and 0.01 eV relative to He_2^+ + He. While it is clear that our low-level calculations of He_3^+ yield much smaller energies than the CCSD(T) results they qualitatively agree. Due to the very weak binding energy of He_3^* and the instability of He_3^+ relative to He_2^+, we did not anticipate observing any trimers from small He_7 clusters. The conditions required to form the trimer are quite precise and it is very rarely (< 0.5%) that the atoms approach slowly enough to form the excited trimer. To form a trimer, the atoms never approach as closely as in the vibrating dimer and all three atoms must contain very low kinetic energies.

4. Stagnation

Stagnation occurs when the initially excited electron does not interact strongly with other atoms, or when the initial excitation is too delocalized to exert any significant force. The first scenario is most likely to occur in trajectories arising from excitation into states very near to the atomic $2s$ and $2p$ excitation energies, which are states at the outer edges of the clusters that have little density inside the cluster.[19] The second possibility most often occurs in very delocalized states which tend to occur at the highest initial excitation energies.

In such trajectories it is not possible to unambiguously determine the end products and so they were simply classified as indeterminate. They are not necessarily completely free of interactions and on a much longer time scale (≫ 1 ps) the majority of the stagnated

trajectories should fully dissociate.

Larger excited helium clusters, He_n^* with $n = 4 - 6$, might be said to exist in a few of the stagnated trajectories, however they are not stable with any finite amount of kinetic energy. These result from very delocalized initial excitations and essentially no motion of the atoms is observed over the length of the computed trajectories. In contrast, the trajectories classified as forming He_2^* and He_3^* all had significant atomic motion and vibrational energy throughout the trajectory.

C. Product distribution

Table I gives the number of trajectories resulting in each of the possible end products. By the end of the calculated trajectories, 90% have dissociated to atoms, 3% to dimers, $< 0.5\%$ to trimers and 7% are stagnant and indeterminate. At 242 fs, stagnated and obviously dissociating trajectories were first allowed to terminate. At $t = 242$ fs just over 91% were classified as fully dissociating and the remaining trajectories were undetermined. Thus only $\approx 1\%$ of the dissociating trajectories from $t = 242$ fs ultimately experienced other interactions and a different fate.

Focusing first on the 87 dimer-forming trajectories, 85% originate from the $8 - 11^{th}$ energy-ordered states. A further 10% arise from states 12 and 13 and the remaining 5% from states 3-7. States 8-14 correspond to the lower energy range of the $2p-$type states, and originate from atoms on the outer edges of the cluster.[19] Only states at the low end of the $2p$ manifold are observed to produce dimers because those at the high energy end of the spectrum either collide with too much energy to remain bound, or have very delocalized states with small forces. Most of the dimers, 82, originate from $p-$type excitations while only 5 occur after excitation into a $2s-$type state.

The character of the dimers at the end of the trajectory is determined by the attachment densities. 43 (49%) of the dimers end in π states, 21 (24%) in σ_s^*, 11 (13%) in π^*, 11 (13%) in σ_s, and 1 (1%) in σ_{p_z}. Vertically excited π states are prohibited from directly forming σ_s dimers as seen from the dimer potential curve (fig. 2). Imagining that all excited states rapidly decay to the lowest energy in the $n = 2$ band, the σ_s state would be highly favored. However, due to symmetry restrictions, 75% of the $n = 2$ dimer states may not directly access the σ_s state, with the result that the slightly higher energy π and σ_s^* states have

much larger populations.

It is not possible to generalize much about the trimers because so few of them are formed. In all trimers the minimal interatomic distance is significantly greater than that observed for the dimers. If the atoms come too close together or with any significant amount of KE the dimer is preferentially formed. Trimers only appear when the atoms approach slowly and the atoms are always more separated than in the dimers. They also do not appear to be fully equilibrated at the end of a 968 fs trajectory.

The end products for most trajectories are rapidly identified considering only the absolute nearest-neighbor (NN) distances. Figure 9a shows the nearest neighbor distance as a function of time for each excited state in the $n = 2$ manifold from one of the initial geometries. It is clear that the majority of the trajectories result in fully dissociated clusters as indicated by the steadily increasing NN distance.

When two atoms collide, their NN distance rapidly decreases and reaches a minimum well below the equilibrium distance of 1.1 Å. All, save one, of the initial geometries had ≥ 1 of its 28 excited states undergo a collision. Dimers as seen in fig. 9 have a periodic NN function and can be identified by multiple minima below 1.1 Å which are separated by similar time intervals. Once formed, most dimers persist until the end of the trajectory. However, there are cases where something occurs, such as a collision of the dimer with another atom, and the dimer ultimately dissociates to He + He*.

To unambiguously identify trimers it is also necessary to consider the second nearest neighbor (2NN) distances. Periodic behavior of both the NN and 2NN distances could result from two separate oscillating dimers, a single trimer, or more generally from larger clusters. The trajectory forms a trimer or larger excited cluster if the NN and 2NN distances are periodic and share a common atom. This occurred in 11 of the 2800 trajectories, and these were inspected individually to be certain that He_3^* was the largest excited cluster. It is unsurprising we did not observe larger clusters because unexcited helium atoms are only bound by weak dispersive forces, which are completely neglected in our calculations, and He_3^* is already barely bound. The trimer is extremely fragile with respect to decomposition into a dimer and an atom and this is also true for larger excited clusters. The case of double dimers requires more energy than is available from the initial excitation and these were observed only when γ_E was chosen to be too large to enforce energy conservation. In principle energy is always conserved, however, because of the finite step sizes used in AIMD

in practice this may not always be true. Furthermore, the possibility of having states with similar character but differing energies, amplifies issues associated with energy conservation.

In the stagnated trajectories with indeterminable final products, the excitation may be very diffuse, or on a non-interacting atom that is separated from the main cluster. As there is no initial kinetic energy the pseudo-stability of the delocalized excitations from states near the upper energy range of the $n = 2$ manifold is due to a lack of any motion. If propagated for much longer times these states may ultimately result in clusters with interesting dynamics but the majority will fully dissociate into atoms. Most commonly, stagnant trajectories arise when the initial excitation that does not significantly interact with other atoms in the cluster. These states contain only weak repulsive forces and eventually all separate into atoms. Stagnation results in nearly unchanging NN distances, however, this is not a sufficient condition to determine that a cluster is stagnate as the other five atoms may still be dissociating.

Figure 9b shows the energies of all states from a single initial geometry. While much of the same information from fig. 9a is contained in this plot, it is also possible to see different final states of the dimer and the very small variations in the energy change for the trimers. Furthermore, it also shows that many of the fully dissociating states are largely parallel, which is consistent with the small number of state changes that arise from these state-following trajectories (90% had ≤ 10 switches).

Overall, no statistically significant correlation was found between the initial geometry and the final products. It was also not possible to reliably predict the end products based on the atomic spread of the vertical excitations or from initial forces. The initial forces are often quite small and slight changes can significantly affect the final outcome. As the CIS forces are likely a bit weaker than the true forces, the ratio of product formation may actually somewhat favor dimers and trimers as more trajectories will experience strong collisions where full dissociation results. The energy and character of the initial states are the crucial factors for predicting the products. Also interesting is the fact that most of the product distribution, and thus the interesting dynamics, occur during the first quarter of the trajectory ≈ 250 fs.

D. Kinetic energy distribution

The maximum total kinetic energy distribution for all clusters is shown in fig. 10. This is the difference in potential energy from the beginning and the end of the trajectories, for all trajectory types. The clusters are launched with zero initial KE, thus, KE can only increase. Most trajectories accumulate very small KEs, although the highest KE values extend to 2 eV. The peak at about 0.7 eV correlates with the energy gap between the atomic $2s$ and $2p$ states. It arises because trajectories initialized and propagated solely on the $2p$ (or $2s$) manifold do not develop significant KE, whereas trajectories which are initialized into a $2p-$type state and transition to a state in the $2s$ manifold will on average gain about 0.7 eV of KE. Note that for excited dimers, this distribution is a poor description because the end of the trajectory is arbitrary in terms of the vibrational period and most of the KE is internal. However, the small number of dimer forming trajectories means they do not significantly affect the overall shape of fig. 10, and they are separately treated in more depth.

The KE distribution, from individual atoms in the fully dissociating clusters at the end of their trajectories, is shown in fig. 11. The maximum amount of KE gained by a single atom is about 0.7 eV which is again the difference between $2s$ and $2p$ states of He. Figure 11 also includes the kinetic energy distribution considering only the atoms which carry all or part of the excitation. These are the atoms preferentially detected in pump-probe experiments. The distributions in fig. 11 are scaled to contain equal area and their mean values are statistically indistinguishable. The excited atom KE distribution contains more atoms in the mid-range, but has fewer atoms with very high or very low kinetic energies than the KE distribution of all the atoms.

The kinetic energies of the final dimers are shown sorted by increasing total KE in fig. 12. Here the KE for each dimer is computed at the potential minimum (1.1 Å), which is the point of maximum internal KE. The internal KE is then taken as the difference in the total and center of mass (COM) KE. The COM KE values are quite low, and it is readily apparent that the primary portion of the dimer KE is from internal energy due to vibrational excitation. The highest energies are around 2 eV, which also corresponds to the potential well depth of the bound σ_s and π dimers (fig. 2). Figure 13 indicates the character of each dimer and shows the internal energy of He_2^* as a function of the vibrational period. The longest periods align with the largest internal energies and arise from π and σ_s states as

may be expected from their broad potential wells (fig. 2). The other types of states are all associated with much shorter periods, and therefore, less vibrational excitation. There are two clear branches in this figure resulting from the difference in the minimum potential energy of the π and σ_s states and the σ_s^* states.

E. Comparison To Experiments

Experimental data on the formation of excited neutral fragments after electronic excitation of helium clusters are scarce. The ejection of Rydberg atoms and molecules from electronically excited He droplets was first detected by the Möller group.[68] The most detailed studies to date employ ultrashort extreme ultraviolet (EUV) pulses to excited large (He_n, $n \geq 10^6$) droplets into electronic bands associated with $n = 3, 4$ manifolds. Neutral intermediates and products are probed by ionization with a second pulse in the infrared (IR) regime that is delayed with respect to the excitation on a femto- to picosecond time scale.[10,11] While the cluster sizes and excitation energy regimes in these measurements differ quite starkly from those discussed here, it is interesting to compare general trends and product formation channels that are evident in both experiment and theory.[11,12,19]

The He_7 clusters studied in this paper primarily undergo full dissociation forming 6 ground state atoms and a single excited atom with a significantly smaller number of trajectories resulting in He_2^* and He_3^*. Experimentally, upon excitation into the $n = 3, 4$ manifolds, atomic ions are also clearly the dominant detected species, accounting for more than 70% of the signal from neutral product ionization.[11] Dimers and trimers comprise most of the remaining contribution to the signal with $< 5\%$ of the total ion signal due to trimers.[11]

We note that the atomic KE distributions calculated here (fig. 11) exhibit a qualitative resemblance with low-energy contributions in experimentally determined Rydberg atom KE distributions. It was previously speculated that these contributions may be due to multibody interactions that were not captured in a simplified cluster excitation model based on an average, repulsive interaction of localized atomic excitations with the surrounding He bath.[11] The results presented here indicate that *ab initio* cluster calculations may be able to unravel some of the physics that is responsible for product channels with low KE release.

The formation of dimers in our calculations proceeds on time scales comparable to the dimer vibrational periods. This is also the time scale that seems to determine the product

distribution. Interestingly, the estimated dimer vibrational periods are all ≤ 250 fs, which is similar to the experimentally observed formation time of excited dimer fragments of 220 fs.[11] While significantly more experimental and theoretical work is needed to understand the intricate coupled electronic and nuclear dynamics in the cluster environment, it is encouraging that several common trends and benchmark values can be recognized in both types of studies.

IV. CONCLUSIONS

The delicate and weak van der Waals attractions that bind helium clusters together are strongly perturbed by electronic excitation of the cluster. In the $n = 2$ manifold, cluster excited states blue-shift relative to the free atom by anywhere from near zero to over 0.5 eV,[19] which is a driving force for at least partial dissociation of the cluster. While there have already been intriguing experimental results probing the fate of excited clusters, there have been no detailed atomistic simulations.[5,9–12] This work begins to fill that gap.

Using small He_7 clusters for computational tractability, we have investigated their fate by *ab initio* molecular dynamics calculations after excitation into the $n = 2$ manifold. On the 1 ps timescale of the simulation, a large majority (90%) of the 2800 trajectories exhibit full dissociation to 6 He + He^*, with kinetic energy releases commensurate with the blue shift discussed above. A small fraction (3%) of the trajectories yield bound excited dimers, as anticipated from the isolated dimer calculations where He_2^* is bound and acts as a He_2^+ core and an outer Rydberg electron. An even smaller fraction ($< 0.5\%$) of trajectories results in trimers. The methods used are not quantitatively accurate, but even if the absolute percentages vary, we anticipate that qualitative conclusions will be mostly unaltered. Higher level theoretical methods incorporating electron correlation or non-adiabatic couplings should not change the facts that a large majority of the clusters will still dissociate and most of the dimer and trimer products will arise from the lowest energy $2p-$type states. For these 7-atom clusters, we did not observe any statistically meaningful correlation between the localization/delocalization of the vertical excitations, and the final products. Nor does the initial localization seem to be strongly correlated with the energy. The most important factors determining the fate of the clusters appear to be the energy and the character (s/p) of the vertical excitation.

In addition to overall statistics, we have reported on the dynamics leading to the different products, through illustrative trajectories. These results suggest the most important dynamics occur during the first 250 fs, indicating that future work with larger clusters may not require as long trajectories as used herein. The dissociation timescale, the kinetic energy release, and the range of products all bear interesting and suggestive similarities to the experimental results for $n = 3, 4$ excitations in clusters four orders of magnitude larger. Caution is needed in such comparisons, of course, not just due to the previously discussed physical differences, but also because of limitations in the trajectory simulations. These include the relatively simple single-excitation treatment of the excited states and use of classical, largely adiabatic state-following trajectories that do not properly treat the quantum nuclei or fully describe non-adiabatic effects. Lacking experimental or more accurate theoretical data, we assessed our method using a higher level of theory for the initial excitations. Another interesting aspect that is not covered by our current results is an explicit time-scale for excitation hopping. Accordingly, the present results leave plenty of opportunity for further work on these fascinating systems.

V. SUPPORTING INFORMATION

Initial geometries and trajectory videos are available as supplementary information.

ACKNOWLEDGMENTS

This work was supported by the Director, Office of Science, Office of Basic Energy Sciences, Chemical Sciences Division of the U.S. Department of Energy under Contract no. DEAC02-05CH11231 and by a National Science Foundation Graduate Student Fellowship.

REFERENCES

[1]R. Fröchtenicht, U. Henne, J. P. Toennies, A. Ding, M. Fieber-Erdmann, and T. Drewello, J. Chem. Phys. **104**, 2548 (1996).

[2]J. P. Toennies and A. F. Vilesov, Ann. Rev. Phys. Chem. **49**, 1 (1998).

[3]J. P. Toennies and A. F. Vilesov, Ang. Chem.-Int. Ed. **43**, 2622 (2004).

[4]M. Y. Choi, G. E. Douberly, T. M. Falconer, W. K. Lewis, C. M. Lindsay, J. M. Merritt, P. L. Stiles, and R. E. Miller, Int. Rev. Phys. Chem. **25**, 15 (2006).

[5]F. Stienkemeier and K. K. Lehmann, J. Phys. B **39**, R127 (2006).

[6]C. C. Wang, O. Kornilov, O. Gessner, J. H. Kim, D. S. Peterka, and D. M. Neumark, J. Phys. Chem. A **112**, 9356 (2008).

[7]D. Pentlehner, J. H. Nielsen, L. Christiansen, A. Slenczka, and H. Stapelfeldt, Phys. Rev. A **87**, 063401 (2013).

[8]D. Buchta, S. R. Krishnan, N. B. Brauer, M. Drabbels, P. O'Keeffe, M. Devetta, M. Di Fraia, C. Callegari, R. Richter, M. Coreno, K. C. Prince, F. Stienkemeier, R. Moshammer, and M. Mudrich, J. Phys. Chem. A **117**, 4394 (2013).

[9]O. Kornilov, C. C. Wang, O. Bünermann, A. T. Healy, M. Leonard, C. Peng, S. R. Leone, D. M. Neumark, and O. Gessner, J. Phys. Chem. A **114**, 1437 (2010).

[10]O. Kornilov, O. Bünermann, D. J. Haxton, S. R. Leone, D. M. Neumark, and O. Gessner, J. Phys. Chem. A **115**, 7891 (2011).

[11]O. Bünermann, O. Kornilov, D. J. Haxton, S. R. Leone, D. M. Neumark, and O. Gessner, J. Chem. Phys. **137**, 214302 (2012).

[12]O. Bünermann, O. Kornilov, S. R. Leone, D. M. Neumark, and O. Gessner, IEEE J. Sel. Top. Quant. Elec. **18**, 308 (2012).

[13]D. Buchta, S. R. Krishnan, N. B. Brauer, M. Drabbels, P. O'Keeffe, M. Devetta, M. Di Fraia, C. Callegari, R. Richter, M. Coreno, K. C. Prince, F. Stienkemeier, J. Ullrich, R. Moshammer, and M. Mudrich, J. Chem. Phys. **139**, 084301 (2013).

[14]G. W. F. Drake and W. C. Martin, Can. J. Phys. **76**, 679 (1998).

[15]D. M. Brink and S. Stringari, Z. Phys. D **15**, 257 (1990).

[16]M. Casas, F. Dalfovo, and A. Lastri, Z. Phys. D **75**, 67 (1995).

[17]A. Viel and K. B. Whaley, Int. J. Mod. Phys. B **17**, 5267 (2003).

[18]M. Ovchinnikov, B. L. Grigorenko, K. C. Janda, and V. A. Apkarian, J. Chem. Phys. **108**, 9351 (1998).

[19]K. D. Closser and M. Head-Gordon, J. Phys. Chem. A **114**, 8023 (2010).

[20]K. von Haeften and K. Fink, Eur. Phys. J. D **43**, 121 (2007).

[21]M. E. Tuckerman, J. Phys. Condens. Matter **14**, R1297 (2002).

[22]J. Hutter, Comp. Mol. Sci. **2**, 604 (2012).

[23]M. Ben-Nun, J. Quenneville, and T. J. Martínez, J. Phys. Chem. A **104**, 5161 (2000).

[24]N. L. Doltsinis and D. Marx, J. Theor. Comput. Chem. **1**, 319 (2002).

[25]A. Castro, M. A. L. Marques, J. A. Alonso, G. F. Bertsch, and A. Rubio, Eur. Phys. J. D **28**, 211 (2004).

[26]I. Tavernelli, U. F. Röhrig, and U. Rothlisberger, Mol. Phys. **103**, 963 (2005).

[27]G. A. Worth, M. A. Robb, and B. Lasorne, Mol. Phys. **106**, 2077 (2008).

[28]B. Lasorne, G. A. Worth, and M. A. Robb, Comp. Mol. Sci. **1**, 460 (2011).

[29]D. R. Yarkony, Chem. Rev. **112**, 481 (2012).

[30]B. F. E. Curchod, U. Rothlisberger, and I. Tavernelli, Chemphyschem **14**, 1314 (2013).

[31]J. C. Tully, J. Chem. Phys. **93**, 1061 (1990).

[32]O. V. Prezhdo and P. J. Rossky, J. Chem. Phys. **107**, 825 (1997).

[33]C. F. Craig, W. R. Duncan, and O. V. Prezhdo, Phys. Rev. Lett. **95** (2005).

[34]J. M. Escartín, P. Romaniello, L. Stella, P.-G. Reinhard, and E. Suraud, J. Chem. Phys. **137**, 234113 (2012).

[35]B. R. Landry and J. E. Subotnik, J. Chem. Phys. **137**, 22A513 (2012).

[36]X. Li, J. C. Tully, H. B. Schlegel, and M. J. Frisch, J. Chem. Phys. **123**, 084106 (2005).

[37]A. L. Sobolewski and W. Domcke, Chem. Phys. Lett. **211**, 82 (1993).

[38]C. A. Mead, J. Chem. Phys. **77**, 6090 (1982).

[39]J. E. Subotnik, S. Yeganeh, R. J. Cave, and M. A. Ratner, J. Chem. Phys. **129**, 244101 (2008).

[40]K. D. Closser and M. Head-Gordon, In Prep. (2013).

[41]D. J. Tozer and N. C. Handy, Phys. Chem. Chem. Phys. **2**, 2117 (2000).

[42]M. Isegawa, R. Peverati, and D. G. Truhlar, J. Chem. Phys. **137**, 244104 (2012).

[43]Y. Shao, L. F. Molnar, Y. Jung, J. Kussmann, C. Ochsenfeld, S. T. Brown, A. T. B. Gilbert, L. V. Slipchenko, S. V. Levchenko, D. P. O'Neill, R. A. DiStasio Jr., R. C. Lochan, T. Wang, G. J. O. Beran, N. A. Besley, J. M. Herbert, C. Y. Lin, T. Van Voorhis, S. H. Chien, A. Sodt, R. P. Steele, V. A. Rassolov, P. E. Maslen, P. P. Korambath, R. D. Adamson, B. Austin, J. Baker, E. F. C. Byrd, H. Dachsel, R. J. Doerksen, A. Dreuw, B. D. Dunietz, A. D. Dutoi, T. R. Furlani, S. R. Gwaltney, A. Heyden, S. Hirata, C.-P. Hsu, G. Kedziora, R. Z. Khaliullin, P. Klunzinger, A. M. Lee, M. S. Lee, W. Liang, I. Lotan, N. Nair, B. Peters, E. I. Proynov, P. A. Pieniazek, Y.-M. Rhee, J. Ritchie, E. Rosta, C. D. Sherrill, A. C. Simmonett, J. E. Subotnik, H. L. Woodcock, W. Zhang, A. T. Bell, A. K. Chakraborty, D. M. Chipman, F. J. Keil, A. Warshel, W. J.

Hehre, H. F. Schaefer, J. Kong, A. I. Krylov, P. M. W. Gill, and M. Head-Gordon, Phys. Chem. Chem. Phys. **8**, 3172 (2006).

[44]W. H. Keesom and K. W. Taconis, Physica **5**, 270 (1938).

[45]S. A. Chin and E. Krotscheck, Phys. Rev. B **52**, 10405 (1995).

[46]D. S. Peterka, J. H. Kim, C. C. Wang, L. Poisson, and D. M. Neumark, J. Phys. Chem. A **111**, 7449 (2007).

[47]J. Harms, J. P. Toennies, and F. Dalfovo, Phys. Rev. B **58**, 3341 (1998).

[48]M. Rosenblit and J. Jortner, J. Phys. Chem. **98**, 9365 (1994).

[49]A. V. Benderskii, R. Zadoyan, N. Schwentner, and V. A. Apkarian, J. Chem. Phys. **110**, 1542 (1999).

[50]J. Eloranta and V. A. Apkarian, J. Chem. Phys. **117**, 10139 (2002).

[51]K. von Haeften, T. Laarmann, H. Wabnitz, and T. Möller, J. Phys. B **38**, S373 (2005).

[52]K. von Haeften, T. Laarmann, H. Wabnitz, T. Möller, and K. Fink, J. Phys. Chem. A **115**, 7316 (2011).

[53]J. B. Foresman, M. Head-Gordon, J. A. Pople, and M. J. Frisch, J. Phys. Chem. **96**, 135 (1992).

[54]D. R. Maurice and M. Head-Gordon, Mol. Phys. **96**, 1533 (1999).

[55]D. Yin and A. D. MacKerell Jr., J. Phys. Chem. **100**, 2588 (1996).

[56]J. Stanton and R. J. Bartlett, J. Chem. Phys. **98**, 7029 (1993).

[57]S. Hirata and M. Head-Gordon, Chem. Phys. Lett. **314**, 291 (1999).

[58]M. A. L. Marques and E. K. U. Gross, Ann. Rev. Phys. Chem. **55**, 427 (2004).

[59]A. Dreuw and M. Head-Gordon, Chem. Rev. **105**, 4009 (2005).

[60]L. Verlet, Phys. Rev. **159**, 98 (1967).

[61]M. Head-Gordon, A. M. Grana, D. R. Maurice, and C. A. White, J. Phys. Chem. **99**, 14261 (1995).

[62]W. C. Martin, Phys. Rev. A **36**, 3575 (1987).

[63]T. van Mourik and T. H. Dunning Jr., J. Chem. Phys. **111**, 9248 (1999).

[64]E. Scifoni, F. A. Gianturco, S. Y. Grebenshchikov, and R. Schinke, J. Chem. Phys. **125**, 164304 (2006).

[65]F. Marinetti, E. Bodo, F. A. Gianturco, and E. Yurtsever, Chemphyschem **9**, 2618 (2008).

[66]S. K. Haldar, B. Chakrabarti, and T. K. Das, Few-Body Syst. **53**, 283 (2012).

[67]P. Barletta and a. Kievsky, Phys. Rev. A **64**, 042514 (2001).

[68]K. von Haeften, A. R. B. de Castro, M. Joppien, L. Moussavizadeh, R. von Pietrowski, and T. Möller, Phys. Rev. Lett. **78**, 4371 (1997).

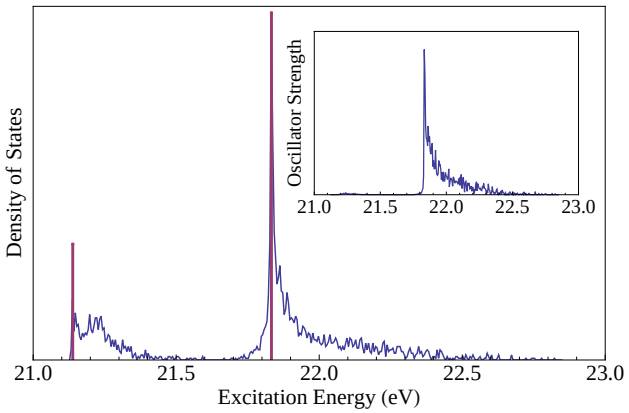

FIG. 1: Density of states in He_7 singlet excited state manifold (100 optimized ground state geometries) with atomic excitation energies marked by vertical lines. The inset shows weighting by oscillator strength.

	Atoms	Dimers	Trimers	Other
242 fs	2536	–	–	264
968 fs	2509	87	11	193

TABLE I: Number of trajectories forming the given products. Most dissociate into individual atoms, with some forming He_2^* and He_3^*. "Other" refers to trajectories which were not classifiable and primarily result from stagnated trajectories.

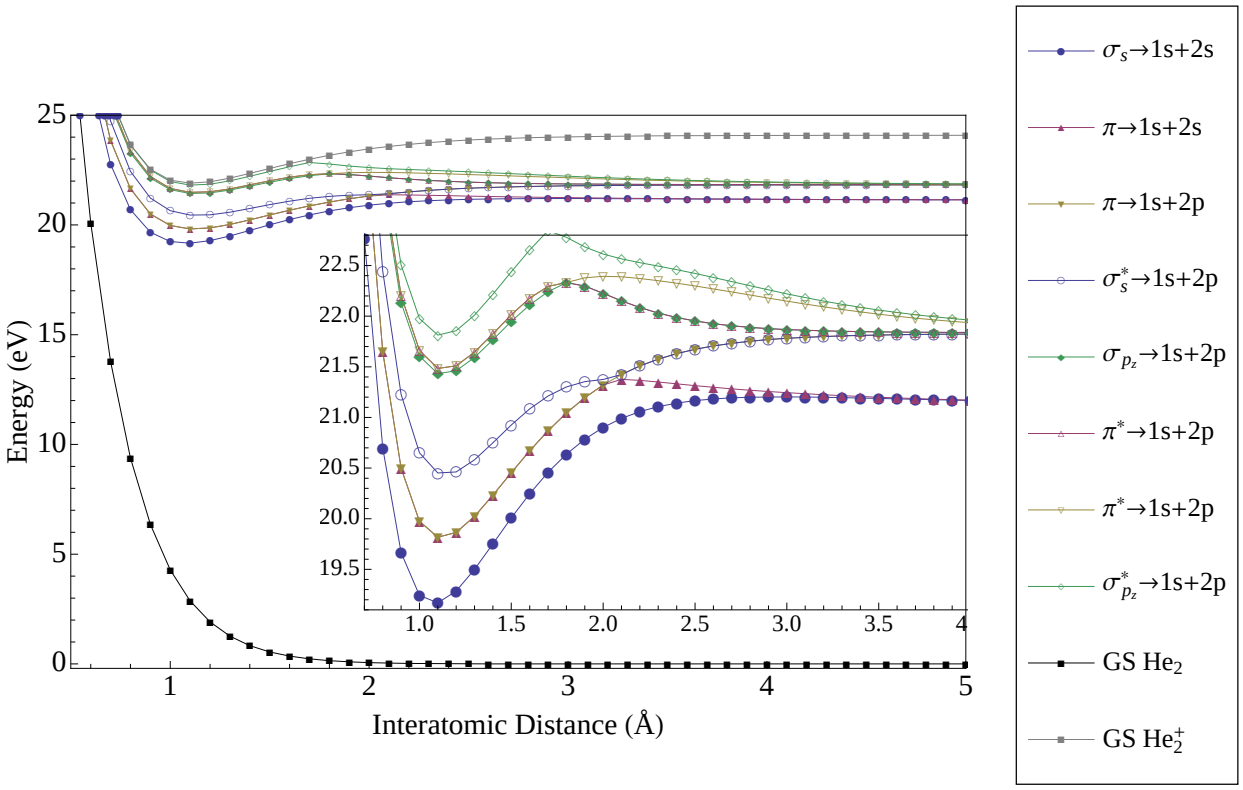

FIG. 2: Potential energy curves of He_2, with CIS/6-311(2+)G. All bound excited states shown have a minimum at ≈ 1.1 Å and four dissociation limits are shown: He $(1s)$+ He $(1s)$, He $(1s)$+ He $(2s)$, He $(1s)$+ He $(2p)$ and $He^+(1s)$+ He $(1s)$. The He_2^* σ_s state nearly parallels the He_2^+ curve except for the slight repulsion in the neutral dimer.

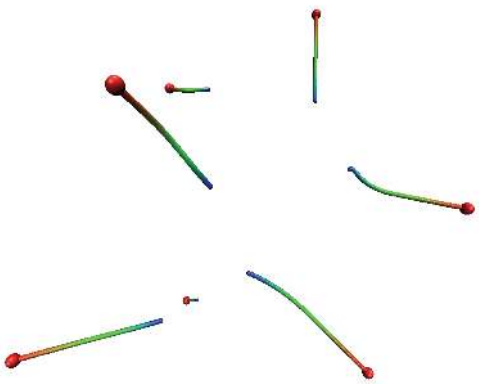

(a) dissociating cluster (7)

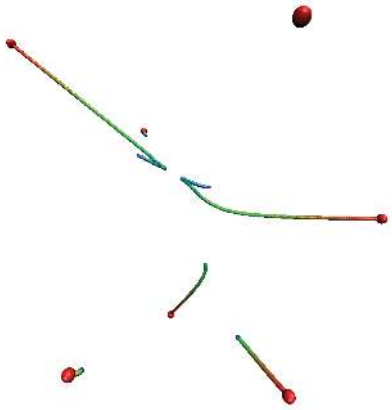

(b) collision (8)

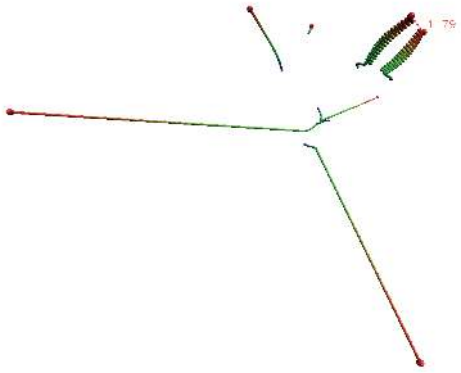

(c) dimer with short period and low vibrational energy (11)

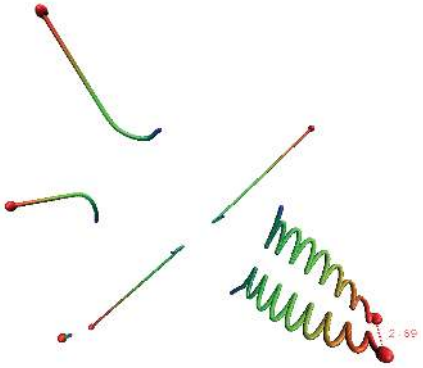

(d) dimer with long period and high vibrational energy (11)

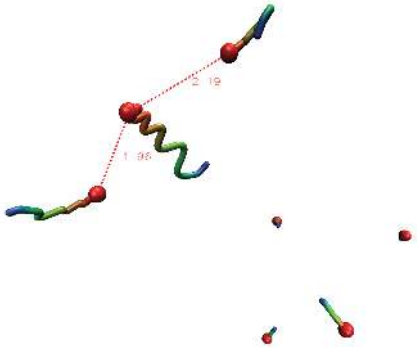

(e) trimer formation (10)

FIG. 3: Sample Trajectories: blue initial point, red (large) final point. The number in parentheses indicates the state populated in the initial excitation and corresponds to the n^{th} excited state in the singlet manifold of He_7.

(a) $t = 0$ fs (b) $t = 121$ fs (c) $t = 181.5$ fs (d) $t = 242, 350.9$ fs

FIG. 4: Attachment/detachment densities for the dissociating trajectory shown in fig. 3a. The detachment (hole) densities are in red and and the attachment (particle) densities are in blue. The initial excitation is into a superposition of $2s$ states and the excitation ultimately ends on a 2s-atomic like state. The excitation moves about until about ≈ 200 fs. Note the atoms are slightly moved between $t = 242$ and $t = 350.9$ fs, but the excitation appears the same.

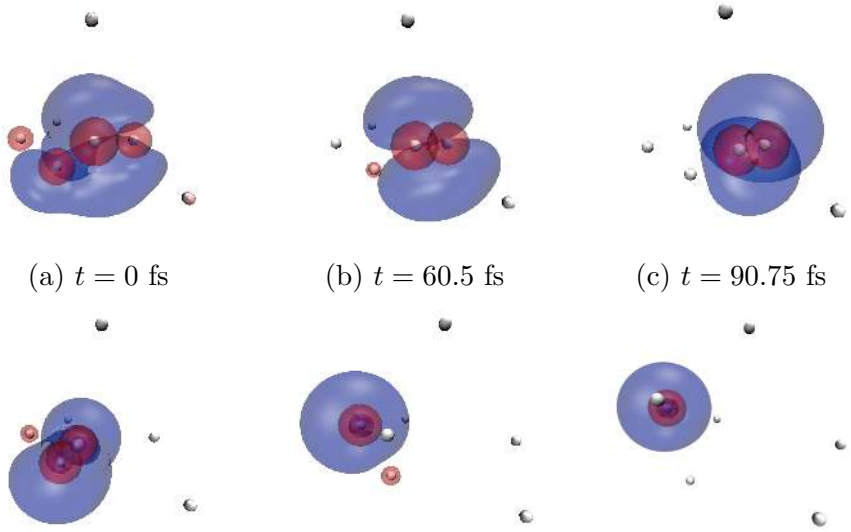

(a) $t = 0$ fs (b) $t = 60.5$ fs (c) $t = 90.75$ fs

(d) $t = 151.25$ fs (e) $t = 211.75$ fs (f) $t = 272.25$ fs

FIG. 5: Attachment/detachment densities for the collision trajectory shown in fig. 3b. The collision occurs between $90 < t < 120$ fs and these plots show the initially delocalized $2p$ superposition state localize onto 2 atoms and end on a single atom after the collision.

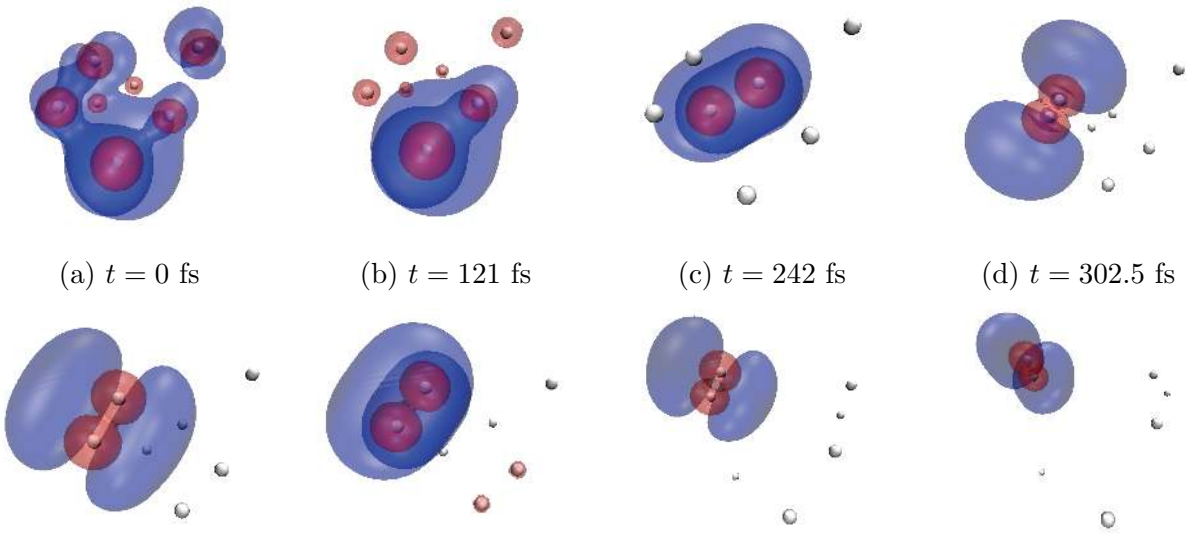

(a) $t = 0$ fs (b) $t = 121$ fs (c) $t = 242$ fs (d) $t = 302.5$ fs

(e) $t = 363$ fs (f) $t = 423.5$ fs (g) $t = 726$ fs (h) $t = 968$ fs

FIG. 6: Attachment/detachment densities for the dimer forming trajectory shown in fig. 3d. The trajectory shows the initially very delocalized $2p-$type state localize onto a dimer at $t \approx 240$ fs and remain there.

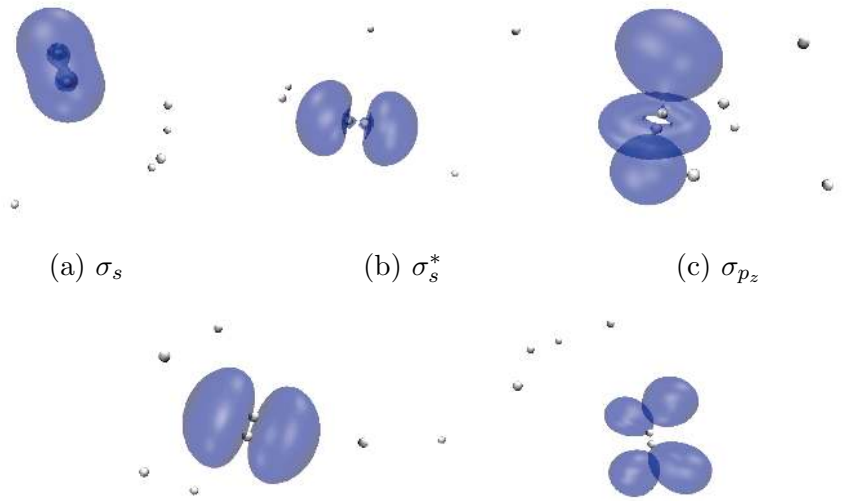

(a) σ_s (b) σ_s^* (c) σ_{p_z}

(d) π (e) π^*

FIG. 7: Attachment densities for each type of stable dimer found in the cluster trajectories. All possible states are observed except the anti-bonding $\sigma_{p_z}^*$ which is barely bound relative to He $(1s)$+ He $(2p_z)$.

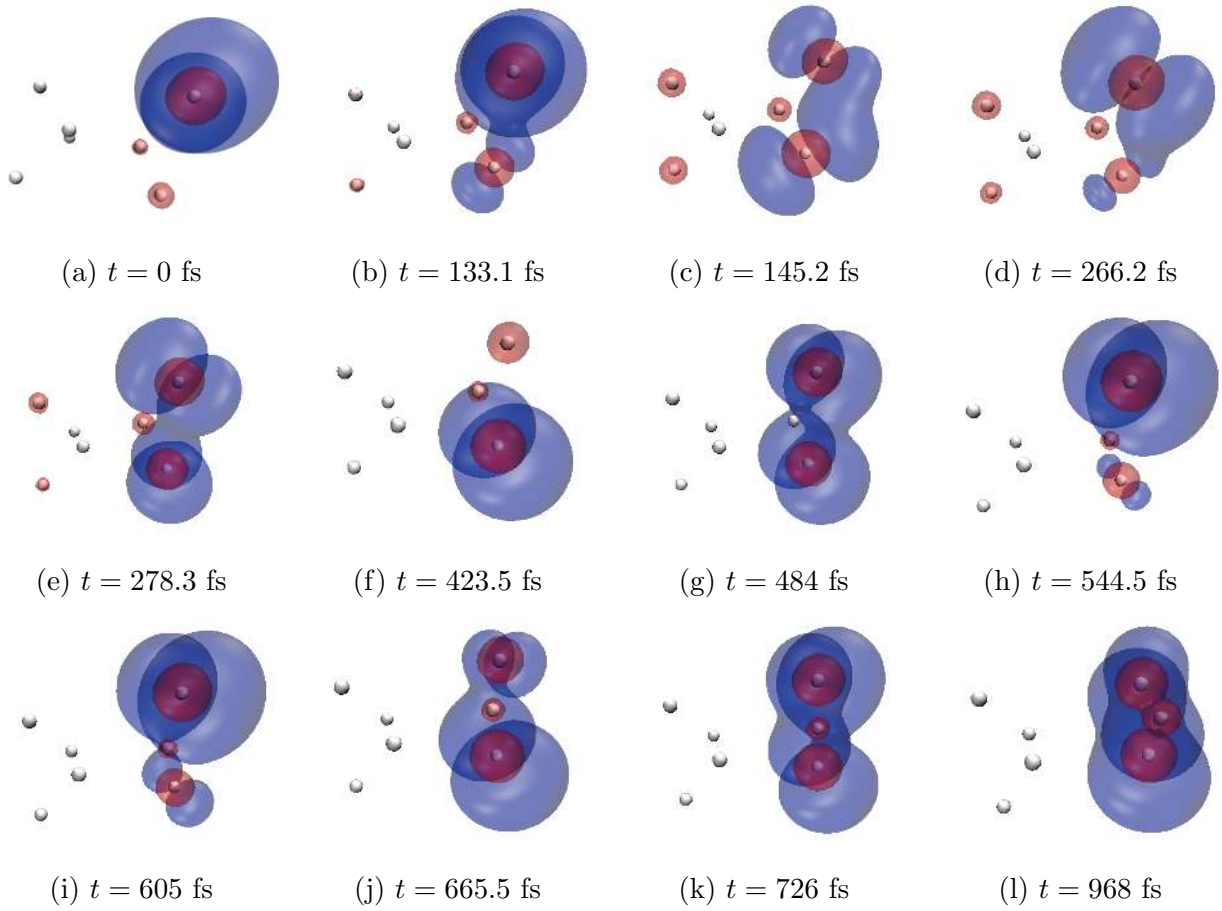

(a) $t = 0$ fs (b) $t = 133.1$ fs (c) $t = 145.2$ fs (d) $t = 266.2$ fs

(e) $t = 278.3$ fs (f) $t = 423.5$ fs (g) $t = 484$ fs (h) $t = 544.5$ fs

(i) $t = 605$ fs (j) $t = 665.5$ fs (k) $t = 726$ fs (l) $t = 968$ fs

FIG. 8: Attachment/detachment densities for the trimer forming trajectory shown in fig. 3e. The initial excitation is into a $2p$ state localized on a single atom and ends in a π-state spread over 3 atoms. At 130 fs the excitation begins spreading to nearby atoms, and then exists for an extended period of time on the two non-adjacent atoms that eventually become the end atoms of the excited trimer.

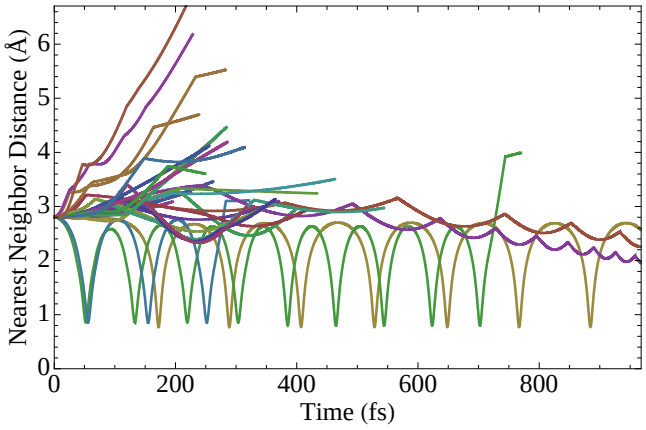

(a) Nearest neighbor distances. Note the periodic oscillation of the dimers and discontinuities due to the formation of trimers. Most trajectories ultimately dissociate but one forms a dimer (periodic, yellow) and two form trimers (discontinuous, brown and purple). Dimers may also be formed transiently as seen by the green trajectory.

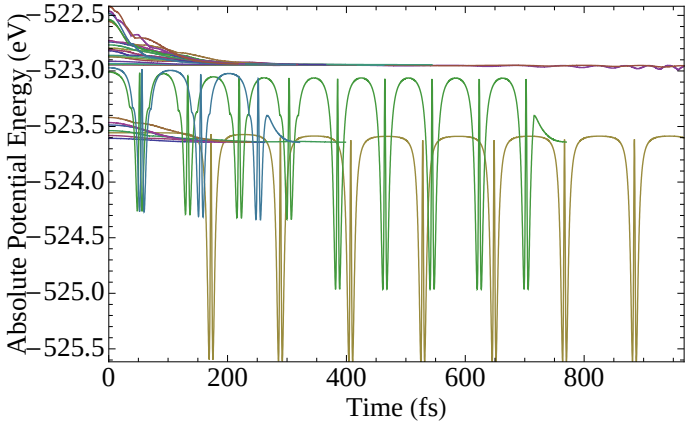

(b) Absolute potential energies. Two primary dissociation limits correspond to $He^*(2s)$+6 He and $He^*(2p)$+6 He, the others are a state from He_2^* and He_3^*. The dimers experience much larger changes in energy and bond length than the trimers.

FIG. 9: Trajectories for each of the 28 states associated with a single initial geometry.

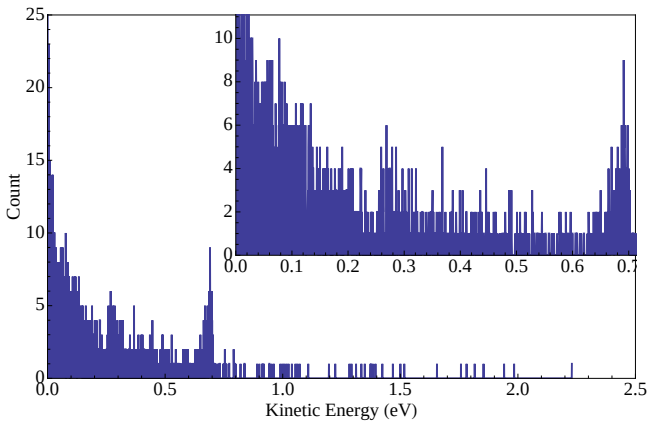

FIG. 10: Kinetic energy of the trajectories at their end point. The total KE is the sum of kinetic energies of all atoms in each cluster. The peak at 0.7 eV is due to relaxation from the $2p$ manifold to the $2s$ manifold.

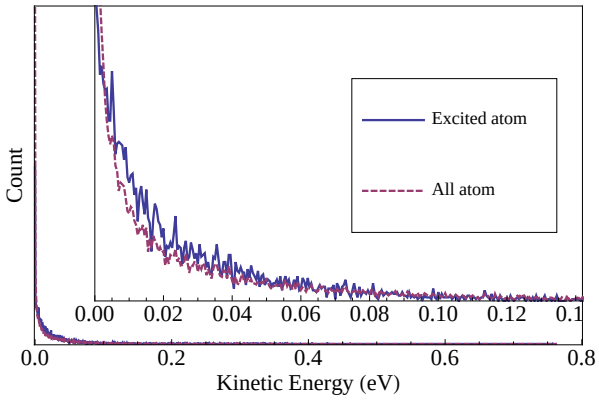

FIG. 11: Kinetic energy distribution of all individual atoms and only the individual excited atoms at the end points of the trajectories. The curves were scaled to equal area.

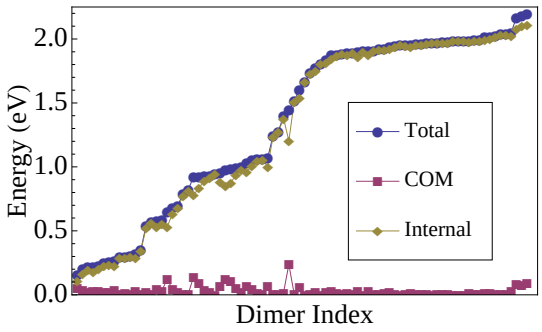

FIG. 12: Kinetic energies of excited helium dimers including center of mass (COM) and internal components. The KE was determined at the potential minimum, which has the maximal KE. The internal KE is the difference of the total KE and the COM KE.

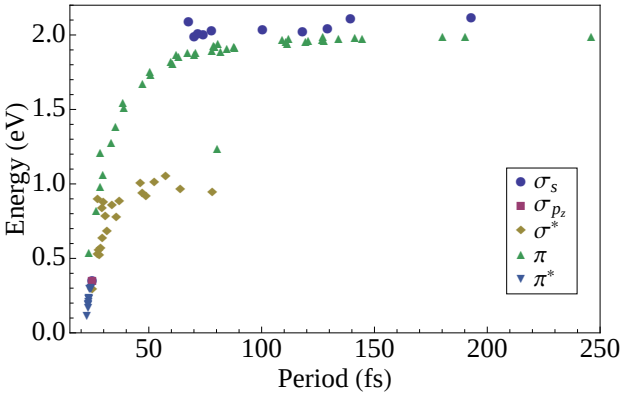

FIG. 13: Period of dimer in femtoseconds vs. the internal energy of the dimer. The variation in period arises from different electronic states and amounts of vibrational excitation.